ab-intio study of anisotropic properties in isomorphic TiX_2 (X=S, Se, Te)

Chhama Pandey[1], Gulzar Ahmed[1], Ramesh Sharma[2] and Yamini Sharma[3*]

[1]*Dept. of Physics, Mewar University, Chittorgarh-312901*

[2]*Dept.of Applied Science, Feroze Gandhi Institute of Engg. and Technology, Raebareli-229001*

[3]*Theoretical Condensed Matter Physics Laboratory, Dept. of Physics, Feroze Gandhi College, Rae Bareli-229001*

Keywords: Titanium dichalcogenides; electronic band structure**;** electron localization functions; phonon band structure; Bader charge partitioning

ABSTRACT

Isomorphic titanium dichalcogenide TiX_2 (X=S, Se, Te) compounds exhibit very diverse and anisotropic chemical and physical properties. The temperature dependent electrical resistivity of $TiSe_2$ was found to exhibit anomalous behavior at low temperatures (< 200 K) which was connected to the emergence of a unique charge density wave (CDW), which was explained on the basis of $2a_0 \times c_0$ superstructure formation, whereas bulk TiS_2 and $TiTe_2$ do not exhibit CDW instability. In order to understand their diverse nature, we have systematically investigated the electronic structure of titanium dichalcogenides by using the FPLAPW and PAW methods based on the density functional theory (DFT). The energy bands calculated by implementing the latest generalized gradient approximation (GGA) with PBE and TB-mBJ potentials confirm the semiconducting nature of TiS_2 and metallic nature of $TiSe_2$ and $TiTe_2$, however the Wu-Cohen potentials show a semi-metallic nature for all three dichalcogenides. The diverse properties of TiX_2 are governed by two bands, S/Se/Te p-band close to the Γ-point and Ti 3d-band around M (L)-points. The presence of electron and hole pockets at the Fermi energy level have been previously confirmed experimentally, although our calculated size and extent of overlap of these pockets was overestimated compared to experiments. Various physical parameters such as electrical conductivity, Seebeck coefficient etc. which depend sensitively on nature of states at the Fermi level also amply illustrate the diversity of the compounds. The electron localization function and Bader charge partitioning illustrate the increasing covalency with varying chalcogenide atom, which is consistent with the spectral features observed in the DOS.

The lattice dispersion of the titanium dichalcogenides are calculated by using the PAW method with PBE potentials. The phonon band structure is correlated to the electronic band structure in order to explain the occurrence of CDW. In $TiSe_2$, the presence of a phonon mode with imaginary frequency indicated lattice instability against distortion. The displacements of Ti-Se atoms of this phonon mode allows the mixing of states of the electron and hole pockets, which leads to lattice distortion i.e. a CDW structure which lowers the energy of the system. Although there is a weak imaginary mode, the mixing of states is absent in TiS_2 due to absence of electron or hole pockets, whereas $TiTe_2$ is structurally most stable.

*Corresponding author email: sharma.yamini62@gmail.com +91-9415117955

1. Introduction

Titanium dichalcogenides TiX_2 (X=S, Se, Te) have been studied extensively, both experimentally and theoretically because of their interesting 2D- layered structure due to which these compounds possess anisotropic physical and thermoelectric properties. Only bulk $TiSe_2$ is known to show phase transition [9, 11, 13] to a modulated crystal structure giving rise to charge density wave (CDW), whereas neither bulk 1T-TiS_2 nor 1T-$TiTe_2$ exhibit any CDW. However, a 2×2 CDW is found to emerge for nanostructures made of less than 4-layers in TiS_2 [35] and only in a single-layer in $TiTe_2$ [36] as observed from angle resolved photoemission spectroscopy and scanning tunneling microscopy studies.

The band structure of TiS_2, $TiSe_2$ and $TiTe_2$ have been measured in great details by angle resolved and temperature dependent photoemission spectroscopy using UV and synchrotron radiations (ARPES) [1-10], neutron diffraction techniques [11], X-rays and polarized X-rays absorption spectroscopy [12-13], infrared reflectivity spectroscopy [14 -15] and time dependent reflectivity spectroscopy [16-17]. Transport properties have also been measured for investigating temperature dependence of the magnetic susceptibility [3, 11], Seebeck coefficient [18], electrical resistivity [7, 11, 19-20] and thermal conductivity [21] of these compounds. The electronic structure of TiX_2 (X=S, Se, Te) has been calculated by numerous methods such as augmented plane wave method (APW) [3], density functional theory-local density approximation-atomic sphere approximation (DFT-LDA-ASA) [6], FLAP [8], reduced Hamiltonian [9], linear combination of atomic orbitals (LCAO) in local density approximation (LDA) [22], rigid band model [23], localized spherical method [24] and full potential linearized augmented plane wave (FP-LAPW) method [25-26].

Some questions however remain unresolved i.e. although the band structures of isomorphic TiS_2 and $TiTe_2$ are similar and show systematic variations, only $TiSe_2$ is known to exhibit a 2×2×2 superlattice which causes CDW transitions at low temperature. Further, it is still questionable whether TiS_2 is a semimetal or an extrinsic semiconductor. In this work, we benchmark our work through comparison with previous work and take it forward to explain the properties of the titanium dichalcogenides on the basis of the derived band structures, density of states (DOS), Bader charge analysis and electron localization functions (ELF). Our calculations will

demonstrate the effect of different exchange-correlation potentials on the structural properties which in turn modifies the electronic structure and thermoelectric properties. It would also be interesting to explore the lattice effects in TiX_2 from the study of phonon dispersion relations, since the origin of CDW in $TiSe_2$ is associated with structural modifications. The phonon modes computed in the high symmetry reference structure are a valuable guide to understanding the dynamical properties of the layered titanium dichalcogenides.

2. Methodology

We have reported the electronic properties of titanium dichalcogenides using the FP-LAPW scheme [27]. The generalized gradient approximation (GGA) Perdew–Burke–Ernzerhof (PBE)-sol [28] and Wu–Cohen (WC) [29] were used for treatment of exchange-correlation effects in the calculations. Additionally, the Tran–Blaha modified Becke–Johnson (mBJ) potential was also employed for electronic and transport calculations since it gives very accurate band gap of solids [30]. For valence states, relativistic effects can be included within a scalar relativistic treatment or with 2nd variational method including spin-orbit coupling. The unit cell is divided into non-overlapping atomic spheres (centre at atomic sites) and an interstitial region. Inside the atomic sphere of radius R_{MT} (MT is the muffin-tin sphere), the basis sets are a linear combination of the product of radial functions and spherical harmonics. In the interstitial region, a plane wave is used. The convergence of this basis set is controlled by a cut-off parameter $R_{MT}K_{max}=7$, where K_{max} is the magnitude of the largest **k**-vectors. The maximum radial expansion l_{max} is set to be 10. The iteration is halted when the difference charge density and energy was less than 0.0001 $e^- a_0^{-3}$ and 0.001 Ry respectively, between steps taken as convergence criterion. The energy cut-off between the core and valence states was set at −6.0 Ry. The thermoelectric properties have been investigated using the program BoltzTrap [31] interfaced with Wien2k which calculates the semi classic transport coefficients. The calculation relies on a Fourier expansion of the band energies where the space group symmetry is maintained by using star functions. Properties such as electrical and thermal conductivities, Hall and Seebeck coefficients etc., can be obtained from the Boltzmann theory and are determined by some micro quantities such as degeneracy of the energy bands near the Fermi level, the effective mass of the charge carriers, the mobility of the charge carriers and the thermal conductivity of phonons. The calculations for TiS_2 were run on a 26×26×13 mesh whereas the transport properties calculations are made on a 57×57×29 mesh. In

$TiSe_2$ and $TiTe_2$ the calculations were performed for 4160 k points on a 20×20×9 mesh, whereas for the transport properties the k-points were increase to 8570 using a dense 59×59×28 mesh.

The vibrational properties were calculated using the projector augmented wave (PAW) method implemented in VASP (Vienna *ab initio* simulation program) [32]. The program calculates the interatomic forces via the Hellmann-Feynman theorem. The direct method used in calculation of phonon spectrum utilizes the interatomic force constant matrix which is derived from a set of calculations on a periodically repeated supercell of a 3×3×3 mesh [33]. All the atoms were put in their equilibrium position initially, and then displaced slightly by +/-0.02 Angstrom. The calculations explore the full BZ for an interaction range of 10.0 Å. A total of 6 single-point energy calculations was run on the supercell containing 56 atoms. The calculations use a plane wave cutoff energy of 400.0 eV with a convergence criterion of 1.00×10^{-5} eV.

3. Results and Discussions:

3.1 Structure:

The ground state properties have been calculated with Ti at 1*a* (origin); and two X atoms at 2*d* (1/3, 2/3, 0.2501) and (2/3, 1/3, –0.2501) [24]. The lattice parameters for TiX_2 (X=S, Se, Te), which has a trigonal crystal structure with space group $P\bar{3}m1$ (164) are given in Table 1. Two layers of close-packed chalcogenide atoms sandwich one metal layer between them i.e. X-Ti-X sandwiches seen in Fig.1a. The inter sandwich binding consists of Ti-atoms contributing 4-electrons from the partially filled 3d-shell and 2-electrons from s-shell ($3d^2 4s^2$) to the two X (S, Se, Te) atoms which constitute the molecular unit TiX_2. The staggered stacking of the two chalcogenide layers forming a slab gives rise to octahedral holes for the metal atoms. In the ideal octahedral arrangement, the c/a ratio (~1.633) is a measure of the cavity size. For TiS_2, $TiSe_2$ and $TiTe_2$, the calculated c/a ratios are 1.699, 1.78 and 1.85 respectively for both WC and PBE-sol potentials, which are overestimated compared to the experimental c/a values of 1.674, 1.698 and 1.725 respectively [14]. The deviation from the ideal ratio is a reflection of strong Ti-X and Ti-Ti bonding. The Ti-X and Ti-Ti bond lengths also increase progressively while going down the VI^{th} group due to decrease in the ionic nature of the chalcogenide ion (Table 1).

Table 1: Parameters of Titanium dichalcogenides TiX_2 (X=S, Se, Te)

Theory	Parameters	TiS_2	$TiSe_2$	$TiTe_2$
FPLAPW-GGA-WC	Lattice parameters (Å)	a=3.3646 c=5.7178	a=3.4797 c=6.1967	a=3.7616 c=6.9864
	Volume(Å)	378.3030	438.5378	577.7459
	Pressure (GPa)	106.7466	83.5119	66.9722
	Bond length (Bohr)	Ti-S=4.5539 Ti-Ti=6.3582 S-S=6.5211	Ti-Se=4.8815 Ti-Ti=6.4842 Se-Se=7.2986	Ti-Te =5.1914 Ti-Ti=6.9857 Te-Te =7.6813
FPLAPW-GGA-PBEsol	Lattice parameters(Å)	a=3.3646 c=5.7178	a=3.4797 c=6.1967	a=3.7616 c=6.9864
	Volume(Å)	378.3030	438.5378	577.7459
	Pressure (GPa)	106.7466	83.5119	66.9722
	Bond length (Bohr)	Ti-S=4.55 Ti-Ti=6.358 S-S=6.5317	Ti-Se=4.794 Ti-Ti=6.575 Se-Se=6.978	Ti-Te =5.266 Ti-Ti=7.108 Te-Te =7.773
PAW-GGA-PBE	**Lattice parameters** (Å)	a=3.3996 c=5.9672	a=3.5183 c=6.1490	a=3.7548 c=6.6990
Experimental lattice parameters [24] (Å)		a=3.407 c=5.6953	a=3.540 c=6.008	a=3.77 c=6.498
Fermi energy (eV)		0.37685	0.40788	0.38695
Cohesive energy(eV)		-13.33	-31.36	-54.37
Formation energy (KJ/mol)		-338.19	-317.79	-204.06

The main difference due to application of different potentials appears in the calculated minimum energy E and the X-X bond lengths. The cohesive energies decrease with varying chalcogenide atoms and have a value of -13.33, -31.36 and -54.37 eV corresponding to TiS_2, $TiSe_2$ and $TiTe_2$ respectively. The formation energies calculated by PAW method are -328.76, -318.67 and -204.6

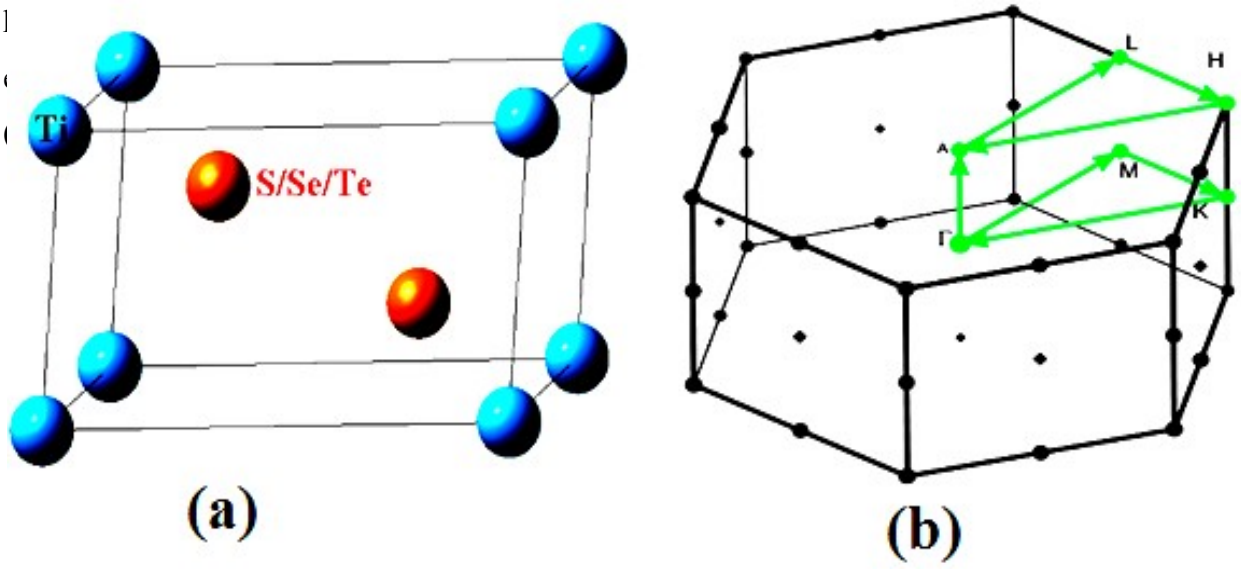

1. (a) Crystal structure (b) Brillouin Zone

3.2.1 Energy bands and Density of states:

The fundamental nature of electronic states in TiS_2 has long been a subject of controversy from both experimental and theoretical points of view. The bulk band structure has been calculated by several authors and experimental literature is also quite extensive. Nevertheless, there is still a controversy whether "ideal" TiS_2 is a semimetal or semiconductor. In numerous previous self-consistent calculations by various methods such as APW [3], FLAPW [8], LSM [17] and FPLAPW [24-25], TiS_2, $TiSe_2$ and $TiTe_2$ have been predicted to be semi metallic. Early optical experiments suggested that both TiS_2 and $TiSe_2$ were semiconducting with a 1-2 eV bandgap. Metallic properties of TiS_2 was supported by resistivity experiment which revealed a T^2 dependence over a temperature range of 4-400 K [19, 20]. Similarly, thermoelectric power measurements by Imai et. al. [38] supported a metallic conduction mechanism. Infrared reflectance spectra measured by Lucovsky et al. also showed TiS_2 to be semi metallic with $10^{22}/cm^3$ charge carriers [14]. Cui et al. predicted semimetal or metallic nature of TiS_2 from ARPES measurements [10] which showed spectral features at very low binding energy at the L-point, however no hole was observed at the Γ-point. From band structure calculated by Suga et al., a bandgap of 0.4 eV was predicted whereas a 0.53 eV experimental bandgap was observed. The general features of their calculated band structures corresponded qualitatively to the photoemission and photoelectron emission microscope results [39]. It is clear from these studies that the actual bandgap is difficult to establish with certainty as it depends sensitively on the fine

details of the crystal structure, so that geometries relaxed with different DFT functionals are associated with different bandgaps. In order to resolve the controversies regarding TiS_2 exhibiting semimetal/semiconductor nature, we performed calculations using GGA-WC and GGA-PBEsol-mBJ exchange-correlation potentials. Energy bands in the vicinity of the Fermi level were examined critically since the topology of bands of TiX_2 compounds is quite similar in nature. We discuss the observed features in the band structures calculated using GGA-WC (Figs. 2) followed by GGA-PBEsol-mBJ (Figs. 3).

The energy bands with been plotted in the energy range –14.0 to 8.0 eV along the high symmetry Γ-M-K-Γ-A-L-H directions in the IBZ are shown in Figs. 2. Our calculated band structures by applying the Wu-Cohen exchange correlation potential are in good agreement with various previous results. The crossing over of bands at Fermi level E_F exhibits the semi metallic character of the three titanium dichalcogenides (the Fermi energy level coincides with 0 eV in Wien2K). On application of latest GGA-PBEsol-mBJ, we observe that a bandgap appears in TiS_2, whereas the band structures of $TiSe_2$ and $TiTe_2$ are modified and continue to exhibit metallic character (Figs. 3).

In the case of TiS_2 (Fig. 2a), the band at Γ-point occurs at 0.398 eV above Fermi energy level, and crosses E_F in the upper layer A-L-H-A of the BZ at the L-point creating a pocket of 0.1792 eV. The presence of a much smaller (3 meV) pocket at L-point was confirmed by high resolution ARPES measurements [10]. Presence of a hole pocket at Γ-point was not observed, which led these authors to confirm the semiconducting nature of TiS_2. For GGA-PBEsol-mBJ calculations, we obtained an indirect bandgap of ~0.126 eV at M-point (in lower layer) and direct bandgap of 0.8 eV at the Γ-point (Fig. 3a). In $TiSe_2$, the first three energy bands at 0.178, 0.280, 0.466 eV crossover from conduction band (CB) to valence band (VB) in the ΓM and ΓK directions and have been labelled Γ_1^c, Γ_2^c, Γ_3^c (Fig. 2b). The figure shows a hole-like band (~0.178 eV) at Γ_1^c which is derived from Se p-states. The energy band at 0.551 eV which is labelled Γ_4^c (which are degenerate at that point), touches the Fermi level (0 eV) at the M-point in the lower Γ-M-K-Γ layer, crosses E_F in the AL and LH directions in the upper A-L-H-A layer, giving rise to an (Ti 3d-states derived) electron pocket of ~0.2539 eV energy at the L point (L_1^v). The experimental

existence of hole-states at Γ-point in $TiSe_2$ was given by Chen et al. [2] from ARPES measurements. Additionally, band structure measurements by Anderson et al. [4] have confirmed that the Γ-point was located 50 meV above E_F and the Ti d-band at L-point located 70 meV below E_F. For the GGA-PBEsol-mBJ potentials, the dispersion of energy bands is modified, two bands at the Γ-point occur at 0.38 eV, and the third band at 0.7 eV (Fig. 3b). Clearly, the calculations with both the exchange-correlation potentials yield hole-pockets which are overestimated compared to experiment. Similarly, in the case of $TiTe_2$, the energy bands at the center of symmetry which occur at 0.280 and 0.44 eV (Fig. 2c), cross the Fermi level along the ΓM and ΓK directions and create hole pockets at the Γ-point. In the upper layer A-L-H-A, an electron pocket of –0.3287 eV is observed at L-point.

Photoelectron spectra measurements have confirmed the presence of electrons in the bands near M(L)-point in the BZ for the three titanium dichalcogenides [3, 4, 10]. From the dispersion of bands in Figs. 2, it is seen that the size of band overlap (GGA-WC) of electron pocket at L-point is ~0.179 eV for TiS_2; 0.43 and 0.608 eV for $TiSe_2$ and $TiTe_2$ respectively. Localized spherical wave (LSW) method using LDA had predicted a 0.7 eV and 0.8 eV overlap for TiS_2 and $TiSe_2$ respectively [24]. The size of hole and electron pockets are observed to increase systematically with decreasing electronegativity of chalcogenide ion. Although the calculated size of hole/electron pockets are grossly overestimated, the various experimental features in $TiSe_2$ and $TiTe_2$ are well described by GGA-WC calculations. Some of these observed features are altered in $TiSe_2$ and $TiTe_2$ due to the application of GGA-PBEsol-mBJ potential, however this exchange-correlation potential better represents TiS_2 and confirms the occurrence of bandgap. Thus, we subscribe to the view of Li et al. and Holt et al. [13, 15] that the electron-hole overlap is significant in understanding the diverse properties of TiX_2, especially the occurrence of instability giving rise to the CDW phenomenon.

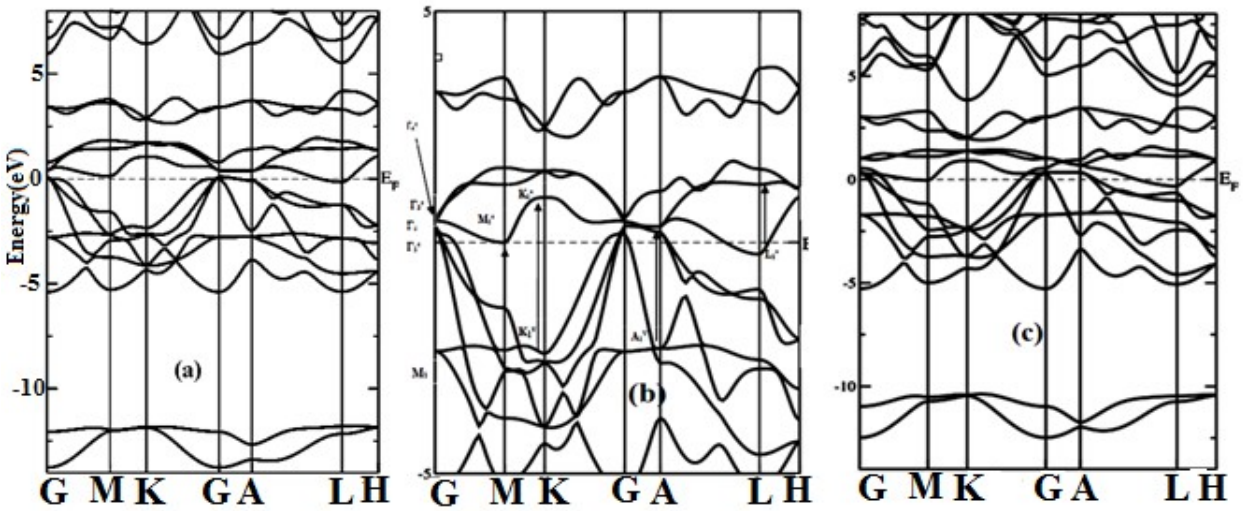

Fig.2 High symmetry energy bands (GGA-Wu-Cohen)

The character of the energy bands can be identified from the partial and total density of states (PDOS and TDOS) in Figs. 3. The main contribution to the states in the vicinity of E_F comes from the hybridization of X (=S, Se, Te) p-orbitals and Ti 3d-orbitals. It is interesting to note that due to changing ionicity, the separation of s- and p-states of the chalcogenide ions varies systematically, i.e. it is largest for the sulphides and smallest for the tellurides (PDOS not shown here). Similarly, there is a change in the shape and position of Ti 3d-states along with an increase in p-d overlap in going down the group from S to Se to Te. The nature of states at the Fermi level is therefore controlled by the hybridization of X p-states and Ti 3d-states. The main contribution to the core states for energies < –10. 0 eV is given by X s-states, whereas the X p- and d- states contribute mainly in the valence region (VB) from –5.3 to E_F. The contribution of s- and p-states of Ti atoms in the valence region is substantially small compared to the d-states. These systematic variations in the DOS are due to the electrostatic interactions between the chalcogen bonding-antibonding p-states of the chalcogenide atom and Ti d-states. These are in turn dependent on the c/a ratio as well as Ti-Ti and Ti-X bond lengths. Thus, the hybridization of s/p-valence bands of the chalcogen-atom and d-conduction band of Ti-atom are of utmost importance for the observed diverse physical properties of TiX_2 compounds.

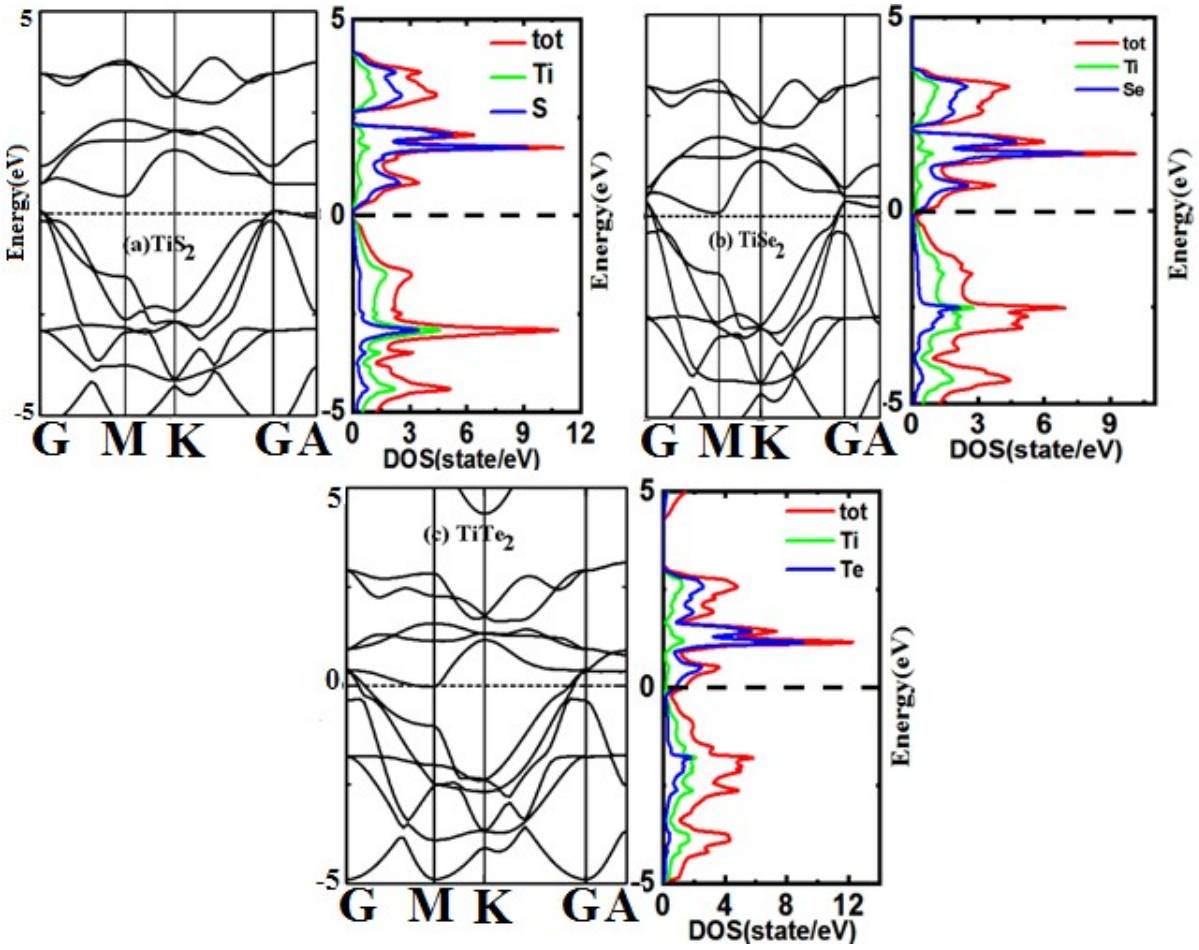

2. High symmetry energy bands and DOS (GGA-PBEsol-mBJ)

3.2.2. Electron Localization Function:

The topological differences in the electronic bands and DOS of the isomorphic compounds in the previous section have amply illustrated that there is a clear dependence of electronic properties on the number of electrons. It would thus be very informative to visualize the electron localization functions (ELF) which is computed by the PAW method using GGA with PBE potentials. The ELF is able to distinguish different bonding situations for electrons compared to plain charge distribution. These functions are related to the likelihood of finding an electron with same spin near a reference point. High values of ELF (close to ~1) are related to the presence of strongly localized electrons. In particular, valuable information regarding the topological aspect of chemical bonding can be provided. The ELF of the TiX_2 compounds along the (101) and (111) planes are presented in such a manner that the planes include the next nearest neighbor atoms

(Figs. 4). In the TiX_2 compounds, the isosurface with highest ELF has a value of 0.8 as seen in the red cores in the chalcogenide atoms with maximum coverage area in the order Te>Se>S, since Te has the largest number of electrons. Smearing of charge is interpreted from the yellow zone with ELF between 0.7-0.8, which is seen to surround the X-atoms. Marginally larger yellow isosurface indicates greater partial localization of S-atoms in TiS_2 compared to $TiSe_2$ and $TiTe_2$. Isosurface of red-yellow (orange) colour (0.75) are also observed surrounding Ti-atoms which varies in intensity with changing chalcogenide atoms. Strongest interaction between S-S atoms leads to greatest distortion from the spherical shape can be observed in the vicinity of S-atom in TiS_2. In the intervening space between Ti-X atoms, aqua to blue isosurface (0.3 to 0.1) covers the greatest area owing to longest bondlength of 2.747 Å (5.1914 Bohr) between Ti-Te indicating greater covalent character. The Te-Te, Se-Se and S-S atoms are bounded as can be seen from the extent of isosurfaces, with greater smearing of aqua/green colour (0.3-0.7) in the space between Te-Te atoms indicating weakest bonds due to largest Te-Te bondlength. The increasing covalency is consistent with the spectral features observed in the DOS (Figs. 3).

The layered structure of TiX_2 and the effect of substitution of X-atoms is clearly observed in the (101) plane. Interestingly, there is appearance of symmetrical small yellow isosurfaces (0.7-0.8) on an aqua (0.2-0.3) background only in the intervening space between Se-Se atoms in $TiSe_2$. These extra ıs behavior of $TiSe_2$ due to

The Bader c ıtion of charge transfer in c -0.81, -0.76, -0.65 e⁻ by t cate that these atoms are sli e can infer the changes in t manifested in the observed ionic systems the electron alent systems, electron den bond lengths vary accordi it being most ionic than ot

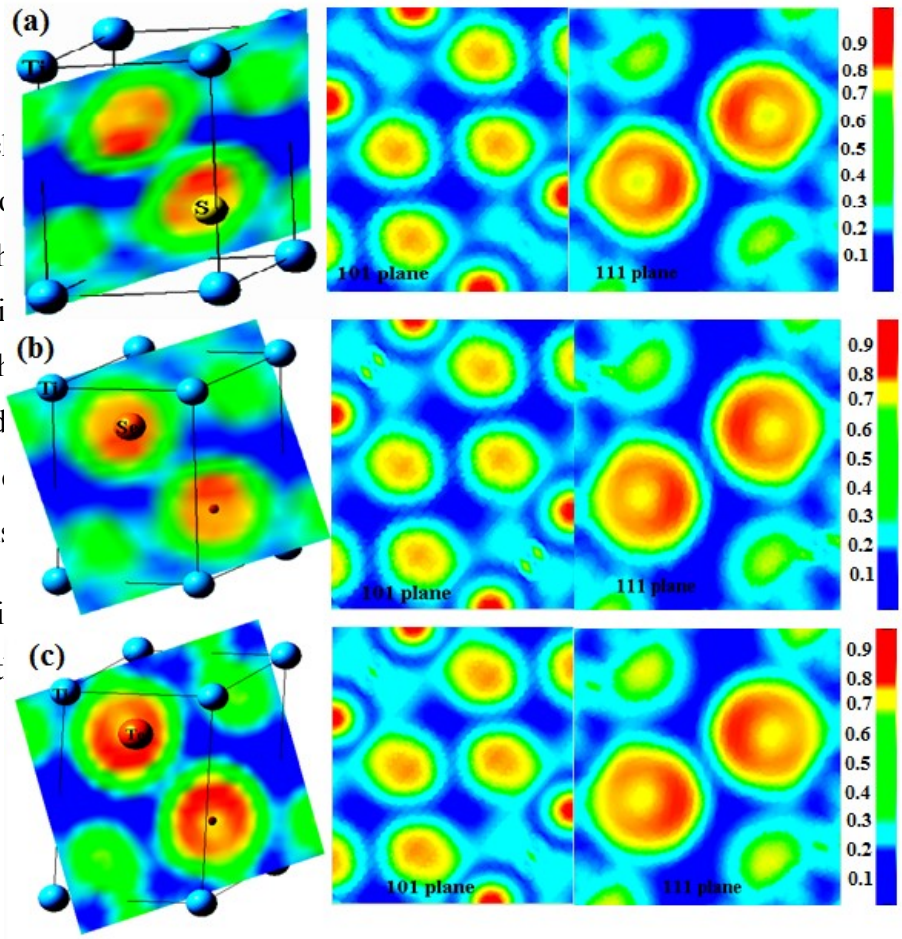

Fig. 4 : Electron localization function for (a) TiS_2 (b) $TiSe_2$ (c) $TiTe_2$

3.3. Vibrational properties:

In the electron diffraction patterns for both TiS_2 and $TiSe_2$, diffuse lines corresponding to $2a_0 \times 2c_0$ superlattice which were characteristic of 1T-crystal and thought to correspond to softening of the L-zone boundary phonon frequency were observed in inelastic neutron scattering data [2]. In order to probe further into the contribution of the lattice and to correlate it to the instability observed only in bulk $TiSe_2$, the vibrational properties are calculated by the force constant method [33].

The phonon frequencies have been calculated within the harmonic approximation and the calculated phonon spectrums are presented along special symmetry directions Γ-L-Z-Γ q-path (Figs. 5). In the harmonic approximation, a crystal is dynamically stable if its potential energy always increases against any combination of atomic displacements. This is equivalent to the condition that all phonon modes have real and +ve frequencies. The signature of a soft phonon

mode, generally called Kohn anomaly was observed by Dolui and Sanvito to occur at the M-point in phonon dispersion modes of titanium dichalcogenides [36]. In Figs. 5, the high symmetry M-point corresponds to the L-point in the upper layer of the BZ (Fig. 1b). The mode with negative value, referred to as the imaginary mode, is observed along the Γ-L branch in TiS_2 and $TiSe_2$ closer to the center of BZ, and may correspond to the Kohn anomaly. All frequencies are real in $TiTe_2$ thereby making it the most stable compound which may be explained from the greater overlap of Te-s/p and Ti-d electrons.

The partial density of phonon states (PDOS) is displayed alongside the phonon band structures in Figs. 5 and provides contributions from each displaced atom. In the case of TiS_2, it is found that phonon modes between 0 and 4.2 THz are essentially dominated by motion of S1-S2 atoms, while the Ti atoms have low contributions to these phonon modes. The high energy phonon modes between 7 to 12 THz are essentially dominated by the displacement of Ti-Ti atoms. In the case of $TiSe_2$, the major contribution to low frequency modes appears to originate from displacements caused by Ti-Se…Ti-Se bonds, whereas the modes in the frequency range 4-6 THz originate from motion of Se1-Se2 atoms. In $TiTe_2$, lower frequency modes from 0-4 THz are caused by motion of Ti-Te bonds and the displacement of Ti-Ti atoms contribute at higher frequencies. The middle modes form a bridge of vibrations between Ti-X atoms. A decreasing trend for the vibrational frequencies is observed as the chalcogen ions size increases. The red shift of modes would reflect weakening of intralayer bonds, while a blue shift suggests enhancement of chemical binding. The soft mode observed along the Γ-L branch in both TiS_2 and $TiSe_2$ gives rise to a small peak in the imaginary frequency regime, this leads to an increase in phonon population in that region which could drive the dynamical instability.

The microscopic origin of CDW phase in transition metal dichalcogenides has been explained either on basis of Fermi surface nesting or excitonic-phononic type mechanism. In case of TiX_2 compounds under consideration here, the origin of CDW instability has been mainly associated with electron-phonon coupling along with interlayer interactions. From our DFT calculations, it may be possible to analyze to some extent how the structural, electronic and vibrational features may explain the CDW instability in bulk $TiSe_2$ and its absence in TiS_2 and $TiTe_2$.

Experimental results and DFT calculations have pointed to charge-carrier dependence as an essential aspect to understand CDW phenomenon in $TiSe_2$. Effects of doping, biaxial strain and

dimensional aspects have been recently investigated by Guster et al. (and references therein) [40]. In section 3.2.2 and Figs. 2, 3, we have observed that in each of the titanium dichalcogenides, the energy bands along the Γ-M direction which are located between 0.5 to 1.0 eV above Fermi level are almost exclusively Ti-atom based and are built from the three t_{2g} orbitals of Ti-atoms (partial DOS not shown here). An hole pocket is created by the band at Γ_4^c which disperses to M-point (L-point) to create an electron pocket in both $TiSe_2$ and $TiTe_2$, whereas in TiS_2 it corresponds to an indirect bandgap for GGA-PBEsol-mBJ potential or absence of electron pocket for GGA-WC potential.

A critical analysis of dispersion of vibrational modes in $TiSe_2$ along the Γ-L (M) direction shows strong dispersion of phonon modes starting from 3.1 THz (53.4 cm^{-1}) at the L-point to converge at a negative frequency of 0.27i THz at the zone center (Fig. 5b). The presence of phonon mode with imaginary frequency indicates that the lattice is unstable against distortion. The specific atomic displacements of Ti and Se atoms of this phonon mode allows the mixing of states at the top of the valence band at Γ-point and bottom of the conduction band at M(L) point and leads to lattice distortion i.e. CDW structure which in turn lowers the energy of the system.

The dispersion of the phonon mode in the Γ-L (M) direction in TiS_2 is comparatively weaker, further the electron or hole pockets are absent, therefore although there is a weak imaginary mode, the mixing of states is absent. On the other hand, in $TiTe_2$, all modes are positive and hence it is structurally most stable. This analysis thus indicates that the CDW instability appears only in bulk $TiSe_2$ and does not occur in bulk TiS_2 and $TiTe_2$. This analysis is also supported by experimental measurements by Baranov et. al. [34] and calculations by tight binding method by Wezal et. al. [35].

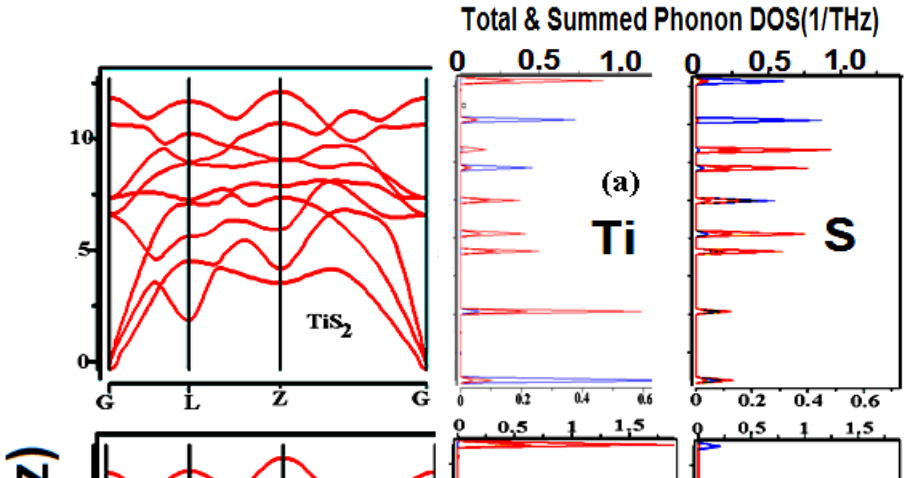

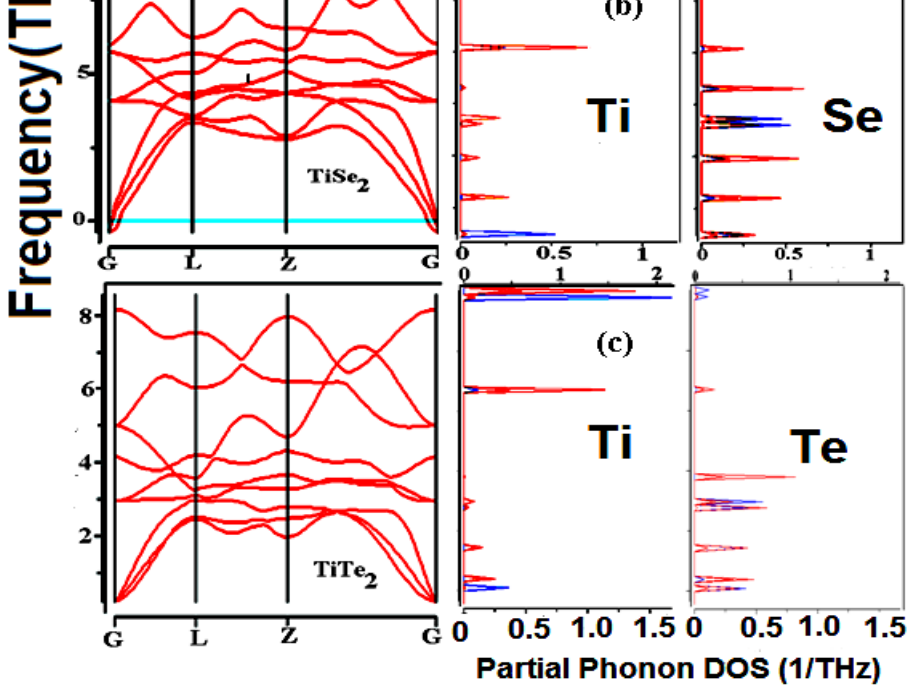

Fig.5 Phonon dispersion curve and Phonon DOS (a) TiS_2 (b) $TiSe_2$ (c) $TiTe_2$

3.4. Transport properties:

From the energy band structures and density of states (Section 3.2.2), it is observed that the TiS_2 exhibits a narrow-gap i.e. indirect semiconductor whereas $TiSe_2$ and $TiTe_2$ exhibit characteristics of a semimetal. A study of temperature dependence of various transport properties would further illustrate the anisotropic behavior of dichalcogenides. The effect of varying the chalcogen ions was therefore investigated by computing the transport properties using the BoltzTraP code in constant relaxation approximation [31]. The Seebeck and Hall coefficients, figure of merit etc. are derived from the numerically evaluated electrical conductivity. The scattering relaxation time of the free carriers of 10^{-14} s initially considered and implemented in the code will be considered here.

Experimental measurements of thermoelectric properties of TiS_2 were made over a wide temperature range from 40 to 300 K. The power factor (PF) of TiS_2 was observed to be large, a feature which is of great advantage in applications as low temperature coolers. A high Seebeck coefficient value of -251μV/K yields a figure of merit ZT of 0.16. The carrier density n was observed to have a value of $\sim 2.8\times10^{20}$ cm^{-3}. These large values were explained by Imai et al. [38] on the basis of the characteristic electronic structure of TiS_2 due to its 2-D structure, and the scattering mechanism (due to occurrence of multiple electron pockets) which gives it an advantage of significantly large PF. The large S values in TiS_2 can be also be explained from the large DOS above and below the E_F, in conduction band (CB) and valence band (VB).

Multivalley structures are observed in the energy bands (Figs. 2 and 3) of the titanium dichalcogenides, with electron pockets around L (M)-point in the hexagonal Brillouin zone (BZ). These structures may be responsible for intervalley scattering which contributes significantly to the transport properties. The various thermoelectric parameters such as Seebeck coefficient, Power factor and figure of merit are plotted against the chemical potential (E_F-μ) for temperatures of 300, 700 and 1200 K in Figs. 6. The chemical potential μ indicates the doping level of the compound, E_F-μ=0 corresponds to chemical potential at Fermi energy level of the compound. For n-type doping, the E_F shifts upwards corresponding to +ve values, and shifts downwards for p-type doping for -ve values. In the case of TiS_2, the Seebeck coefficient is greatly enhanced in a narrow region around E_F-μ=0, which indicates that quite a high value of (-ve) S can be achieved through a small n-type doping at 300 and 700 K. The value of Seebeck coefficient is highest at 700 K for pure TiS_2 at E_F, i.e. μ=0. Maximum $|S|$ lies within a small chemical potential region for ambient as well as high temperature n-type or p-type doping. In $TiSe_2$ and $TiTe_2$, the largest S lies in the -ve μ region away from the Fermi level and does not show too much of temperature dependence in $TiSe_2$. In $TiTe_2$, the value of S is highest at very high temperature (1200 K), and appears to be temperature dependent for -ve value of μ. The Seebeck coefficient is greatly enhanced in both the materials for high level of n-type doping at +ve chemical potentials far away from E_F.

Large values of $|S|$ leads to large power factor for both n-type and p-type doping, with p-type doping performing better at all temperatures in TiS_2 (calculated value of 11.4 $\mu W/K^2cm$ at ambient temperature is underestimated compared to experiment [38]). Power peaks are lowest at

ambient temperature and highest at 1200 K following the same trends as observed in Seebeck coefficient $|S|$.Power factor for $TiSe_2$ for -ve value of μ (p-type) is higher than that for n-type doping, whereas values for $TiTe_2$ are quite low compared to TiS_2 and $TiSe_2$. Surprisingly, a high sharp peak at 300 K is observed for n-type doping far away from E_F. The figure of merit ZT= $S^2\sigma T/(\kappa ¿¿e+\kappa_L)¿$ is independent of the relaxation time, and presents the combined effects of electrical conductivity, electronic component of thermal conductivity and Seebeck coefficient. The figure of merit in our calculations is calculated for the κ_e component. In the vicinity of E_F, ZT for TiS_2 shows similar trends for both positive and negative chemical potentials. The value is maximum (0.7) for n-type doping at 300 K and a similar maximum for p-type doping at 700 K. A smaller peak it 0.42 is observed at Fermi level at ambient temperature. Our calculated value is overestimated compared to experimental ZT~0.16 [38].

The calculated transport properties of the isomorphic titanium dichalcogenides at ambient temperature are presented in Table 2. It is possible to appreciate the difference in values of the transport parameters due to the application of GGA-WC and GGA-PBEsol-mBJ potentials. The Seebeck coefficient, figure of merit, thermal and electrical conductivity are plotted in Figs. 7. The anisotropic behavior due to semiconducting nature of TiS_2 which have a high Seebeck coefficient, low electrical and thermal conductivity and high figure of merit as well as the metallic nature of $TiSe_2$ and $TiTe_2$ are clearly illustrated.

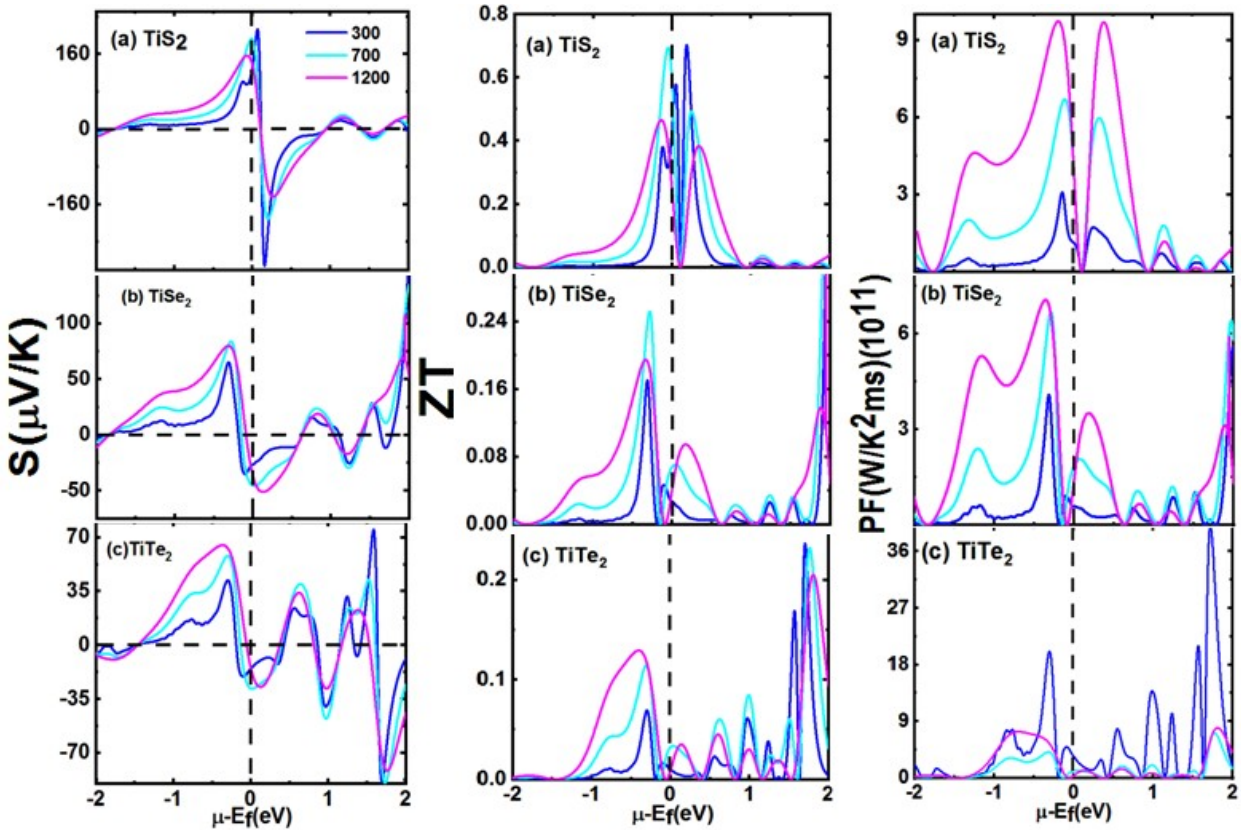

6. Transport properties with chemical potential

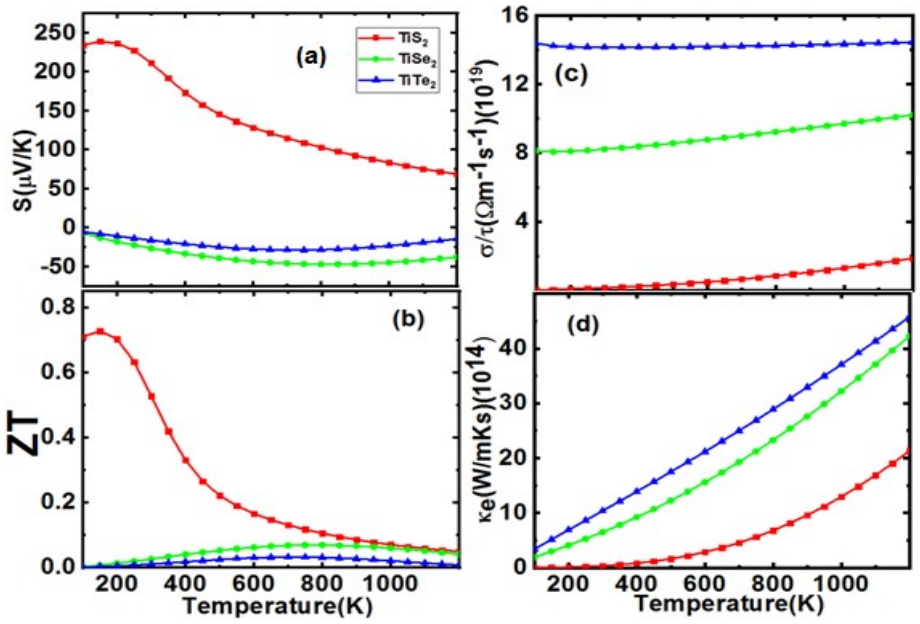

7. Temperature dependent Transport properties of TiX_2

Table 2: Transport parameters of Titanium Dichalcogenides (300 K)

	Ex-Correlation Potential	S (μV/K)	Power factor (10^{10}) (W/ K^2m)	ZT	σ(10^{19}) (1/Ωm)	ρ (Ωm)	n (1/cm^3)
TiS_2	GGA-PBEsol-mBJ	212.0	6.44	0.4274 0.16 [38]	0.1439	0.14×10^{-4}	7.82×10^{19}
	GGA-WC	19.36	11.14 (10^9)	0.011217	0.29	3.44×10^{-5}	1.7×10^{21}
$TiSe_2$	GGA-PBEsol-mBJ	-26.15	5.62	0.02592	8.22	0.012×10^{-6}	7.81×10^{22}
	GGA-WC	-1.76	0.354 (10^9)	0.000121	1.14	0.877×10^{-6}	4.11×10^{22}
$TiTe_2$	GGA-PBEsol-mBJ	-15.85	3.56	0.01028	14.16	0.7×10^{-6}	9.2×10^{21}
	GGA-WC	-3.86	2.48 (10^9)	0.000539	1.83	0.546×10^{-6}	1.04×10^{22}

4. Conclusions:

A theoretical investigation of the electronic behavior gives us a comprehensive understanding of the transition metal dichalcogenides. Our calculations based on the FP-LAPW method using various exchange-correlation potentials with GGA are able to illustrate to some extent the diverse properties of the TiX_2 compounds. Contradictions regarding the semi-metallic or semiconducting nature of TiS_2 are removed, the GGA-PBEsol with mBJ potential accounts well for the observed semiconducting properties of TiS_2 with an indirect band gap of 0.126 eV. At energies near E_F, $TiSe_2$ and $TiTe_2$ were observed to be governed mainly by two bands, a hole-like Se/Te p-band close to the Γ-point and Ti 3d-band around L (M)-point. The s-p orbital separation for the chalcogenide ion is reduced while going down the group i.e. Te<Se<S, whereas p-d overlap is greatest in $TiTe_2$. The GGA-WC potential is adequate to correctly describe the electronic properties of $TiSe_2$ and $TiTe_2$, although the electron and hole pockets are overestimated compared to ARPES studies.

From the ELF and Bader charge partitioning, the changes in the ionic or covalent contributions in the Ti-X, X-X bonds are clearly manifested in the spatial distribution of the electron density. The isosurface with highest ELF around the X-atoms indicates that the atoms are localized. Strongest interaction between S-S atoms leading to greatest distortion from the spherical shape can be observed in the vicinity of S-atom in TiS_2. The shortest Ti-S distance is also consistent with it being most ionic.

The reason that CDW instability appears only in bulk $TiSe_2$ and does not occur in bulk TiS_2 and $TiTe_2$ was analysed in terms of dispersion of vibrational modes along the Γ-L (M) direction. In $TiSe_2$, the presence of a phonon mode with imaginary frequency indicates lattice instability against distortion. The displacements of Ti and Se atoms of this phonon mode allows the mixing of states at the top of the valence band at Γ-point and bottom of the conduction band at M(L) point which leads to lattice distortion i.e. CDW structure which lowers the energy of the system. Although there is a weak imaginary mode, the mixing of states is absent in TiS_2 due to absence of electron or hole pockets, whereas $TiTe_2$ is structurally most stable.

The diverse properties of the titanium dichalcogenides with semiconducting or semi metallic behaviour has been illustrated through the energy bands and density of states. The 2D electron density presented as electron localization function shows the mixed ionic-covalent nature of TiX_2 which clearly depends on the X-X and Ti-X bond lengths. Since the Seebeck coefficient and

electrical conductivity are most sensitive to the nature of energy bands in vicinity of the Fermi level, the calculated transport properties also illustrate the anisotropy of the titanium dichalcogenides.

Acknowledgements

We are grateful to Prof. Blaha and his team for the WIEN2k code and Prof. Hafner and his team for the VASP code.

References

[1] M. M. Traum, G. Margaritondo, N. V. Smith, J.E. Rowe and F. G. Di Salvo, *Phys. Rev. B.* **1978**, **17,** 1836-1838.

[2] C. H. Chen, W. Fabian, F.C. Brown, K. C. Woo, B. Davies, B. DeLong and A.H. Thompson, *Phys. Rev. B.* **1980**, 21, 615-624.

[3] D. K. G. de Boer, C. F. van Bruggen, G. W. Bus, R. Coehoorn, C. Hass, and G. A. Sawatzky, *Phys. Rev. B.* **1984,** 29, 6797-6809.

[4] O. Andersen, R. Manzke and M. Skibowski*, Phys. Rev. Let*. 1985, 55, 2188-2191.

[5] S. Harm, R. Durig, R. Manzke, M. Skibowski, R. Claessen and J. W. Allen, *J Elec. Spec. and Rel. Phen.,* **1994***,* 68, 111-119.

[6] R. Claessen, R. O. Anderson, G-H. Gweon, J. W. Allen, W. P. Ellis, C. Janawitz, C. G. Olson, Z. X. Shen, V. Eyert, M. Skibowski, K. Friemelt, E. Bucher and S. Hufner, *Phys. Rev. B.* **1996**, 54, 2453-2464

[7] L. Perfetti, C. Rojas, A. Reginelli, L. Gavioli, H. Berger, G. Margaritondo, M. Grioni, R. Gaal, L. Forro and F. R. Albenque, *Phys. Rev. B.* **2001**, 64, 115102-1-8.

[8] P. Aebi, Th. Pillo, H. Berger and F. Levy, *J. Elec. Spec. and Rel. Phen.,* **2001**, 117, 1-17.

[9] T. E. Kidd, T. Miller, M. Y.Chou and T. -C. Chiang, *Phys. Rev. Let.*, **2002**, 88, 226402-1-4

[10] X. Y. Cui, H. Negishi, A.N. Titov, S.G. Titov, M. Shi and L. Patthey, *Phys. Rev. B.* **2006**,73, 85111-85116.

[11] F. J. Di Salvo, D. E. Moncton and J. V. Waszczak, *Phys. Rev. B.* **1976,** 14, 4321-4328.

[12] S. Bocharov, G. Drager, and D. Heumann, S. Simunek and O. Sipr, *Phys. Rev. B.* **1998**, 58, 7668-7674.

[13] M. Holt, P. Zschack, H. Hong, M. Y. Chou and T. -C. Chiang, *Phys.Rev. Let.* **2001**, 86,

3799-3801.

[14] G. Lucovsky, R. M. White, J. A. Benda and J. P. Revelli, *Phys. Rev. B.* **1973**, **7**, 3859-70.

[15] G. Li, W. Z. Hu, D. Qian , D. Hsieh, M. Z. Hasan , E. Morosan, R. J. Cava and N. L. Wang, *Phys. Rev. Let.* **2007**, 99, 27404-1-4.

[16] C. M. Julien, Proc. Int. Wshp" Ad Tecq Eng. Sources Inv. Testing" (2004) L2-1-18.

[17] E. Mohr-Vorobeva, S. L. Johnson, P. Beaud, U. Staub, R. De Souza, C. Milne, G. Ingold, J. Demsar, H. Schaefer and A. Titov, *Phys. Rev. Let.*, **2011**, 107, 36403-1-4.

[18] A. Amara, Y. Frongillo, M.J. Aubin, S. Jandl, *Phys. Rev. B.* **1987**, 36, 6415-6419.

[19] A. H. Thompson, *Phys. Rev. Let.* **1975**, 35, 1786-1788.

[20] A. H. Thompson, K. R. Pisharody and R. F. Koehler, *Phys. Rev. Let.* **1972**, 29, 163-166.

[21] C. Ayache and M. Nunez-Regueiro, *J. de. Phys.* **1981**, 42, 338-340.

[22] A. Zunger and A. J. Freeman, *Phys. Rev. B.* **1978**, 17, 1839-1842.

[23] M. Kertesz and R. Hoffmann, J. Am. Chem. Soc. **106** (1984) 3453-3460.

[24] C. M. Fang, R. A. de Groot, and C. Hass, *Phys Rev B.* **1997**, 56, 4455-4463.

[25] A. H. Reshak and S. Auluck, *Phys. Rev. B.* **2003**, 68, 245113-1-7.

[26] A. H. Reshak, I. V. Kityk, and S. Auluck, *J. Chem. Phys.* **2008**, 129, 074706-1-5.

[27] P. Blaha, K. Schwarz, G. K. H. Madsen, D. Kvasnicka and J. Luitz, WIEN2k (Vienna University of Technology, Vienna, Austria 2001).

[28] Z. Wu and R. E. Cohen, *Phys. Rev. B.* **2006**, 72, 235116-6.

[29] J. P. Perdew, K. Burke and M. Ernzerhof, Phys. Rev. Lett. **77**, 3865 (1996).

[30] F. Trans and P. Blaha, Phys. Rev. Lett. 102 (2009) 226401

[31] G. K. H. Madsen and D. J. Singh, *Comp. Phys. Comm.* **2006**, 175, 67- 71.

[32] G. Kresse and J. Hafner, *Phys. Rev. B.* **1993**, 47, 558; *Phys. Rev. B.* **1994**, 49 14251; G. Kresse and J. Furthmüller, *Comput. Mat. Sci.*, **1996,** 6, 15; G. Kresse and J. Furthmüller, *Phys. Rev. B.* **1996**, 54, 11169.

[33] K. Parlinski, Z. Q. Li and Y. Kawazoe, *Phys. Rev. Let.* **1997**, 78, 4063-4072.

[34] N. V. Baranov, K. Inoue, V. I. Maksimov, A. S. Ovchinnikov, V. G. Pleschov, A. Podlesnyak, A. N. Titov and N. V. Toporova, *J. Phys.: Condens. Mat.* 2004, 16, 9243-9258.

[35] J. van Wezel, P. N-Williamson and S. S. Saxena, *Phys. Rev. B.* **2010**, 81, 165109

[36] K. Dolui and S. Sanvito, *Europhys Lett.* 1115 (2016) 47001-3

[37] P. Chen, W.W. Pai, Y.-H. Chan, A. Takayama, C.-Z. Xu, A. Karn, S. Hasegawa,

M.Y. Chou, S.-K. Mo, A.-V. Fedorov and T.-C. Chiang, Nature Commun., 8 (2017) 516

[38] H. Imai, Y.Shimakawa and Y.Kubo, Phys. Rev. B 64 (2001) 241104

[39] S. Suga, C. Tusche, Y-ichiro Matsushita, M. Ellgith, A. Irizawa, J. Krischner, New J. Phy. 17 (2015) 083010

[40] B. Guster, E. Canadell, M. Pruneda and P. Ordejon, 2D-materials, 5 (2018) 025024

Figure captions

1. (a) Crystal Structure of TiS_2
   (b) Irreducible Brillion zone (IBZ) of CdI_2 type crystal with high symmetry points Γ-M-K-Γ-A-L-H
2. Energy Bands (a) TiS_2 (b) $TiSe_2$ (c) $TiTe_2$ along high symmetry points Γ-M-K-Γ-A-L-H (GGA-Wu-Cohen potential)

3. Energy Bands and Density of States (a) TiS_2 (b) $TiSe_2$ (c) $TiTe_2$ along high symmetry points Γ-M-K-Γ-A (GGA-PBEsol-mBJ potential)

4. Electron Localization Function of TiX_2along [100] and [111] planes

5. Phonon dispersion curves and Phonon DOS of (a) TiS_2 (b) $TiSe_2$ (c) $TiTe_2$

6. Variation with chemical potential (E_F-μ) (i) Seebeck Coefficient (ii) Figure of merit Z (iii) Power factor for TiX_2

7. Temperature dependence of (a) Seebeck Coefficient (b) Electrical conductivity (c) Figure of merit (d) Thermal conductivity for TiX_2

Table captions:

1. Parameters of Titanium dichalcogenides TiX_2 (X=S, Se, Te)
2. Transport properties of Titanium dichalcogenides (300 K)